Available online at www.sciencedirect.com
ScienceDirect
Journal of Solid State Chemistry 179 (2006) 3615–3627
JOURNAL OF SOLID STATE CHEMISTRY
www.elsevier.com/locate/jssc

Synthesis and characterization of two new photochromic organic–inorganic hybrid materials based on isopolyoxomolybdate: $(HDBU)_3(NH_4)[\beta\text{-}Mo_8O_{26}]\cdot H_2O$ and $(HDBU)_4[\delta\text{-}Mo_8O_{26}]$

Violaine Coué, Rémi Dessapt, Martine Bujoli-Doeuff, Michel Evain, Stéphane Jobic*

Institut des Matériaux Jean ROUXEL, UMR 6502 CNRS—Université de Nantes, Laboratoire de Chimie des Solides, 2 rue de la Houssinière, BP 32229, 44322 Nantes Cedex 3, France

Received 26 April 2006; received in revised form 11 July 2006; accepted 23 July 2006
Available online 27 July 2006

Abstract

Two new organic–inorganic hybrid compounds of molybdenum(VI) $(HDBU)_3(NH_4)[\beta\text{-}Mo_8O_{26}]\cdot H_2O$ **1** and $(HDBU)_4[\delta\text{-}Mo_8O_{26}]$ **2** have been synthesized and characterized by elemental analyses, FT-IR and UV–vis spectroscopies, and single-crystal X-ray diffraction (at 293 and 100 K, respectively). Compound **1** is obtained at room temperature by adding 1,8-diazabicyclo[5.4.0]undec-7-ene (DBU) on aqueous molybdate solution at pH = 5.7. Compound **2** is obtained hydrothermally from **1** (110 °C, 24 h, autogenous pressure). Compound **1** crystallizes in the triclinic crystal system, space group $P\bar{1}$, with $a = 11.2492(9)$, $b = 14.1907(10)$, $c = 16.7498(10)$ Å, $\alpha = 80.993(4)$, $\beta = 72.272(6)$, $\gamma = 71.696(7)^\circ$, $V = 2412.5(3)$ Å^3 at $T = 20$ °C and $Z = 2$. The refinement of the structure leads to a residual factor $R = 0.0697$ for 10234 independent observed reflections $[I/\sigma(I) \geqslant 2]$ and 623 parameters. Compound **2** crystallizes in the triclinic crystal system, space group $P\bar{1}$, with $a = 11.3158(9)$, $b = 11.3773(8)$, $c = 13.2884(17)$ Å, $\alpha = 92.110(8)$, $\beta = 112.127(9)$, $\gamma = 117.581(7)^\circ$, $V = 1357.4(3)$ Å^3 at $T = -173$ °C and $Z = 2$. The refinement of the structure leads to a residual factor $R = 0.0226$ for 11812 independent observed reflections $[I/\sigma(I) \geqslant 2]$ and 354 parameters. The structure of **1** consists of β-$[Mo_8O_{26}]^{4-}$ anions with $HDBU^+$ and NH_4^+ cations connected to the mineral parts by hydrogen bonds and the structure of **2** contains δ-$[Mo_8O_{26}]^{4-}$ anions with $HDBU^+$ counter-cations. Both the thermal and chemical isomerizations of the two $[Mo_8O_{26}]^{4-}$ isomers are highlighted and discussed. Photochromic behaviors of compounds **1** and **2** are also reported.

Keywords: Organic–inorganic hybrid materials; Polyoxometalates; DBU; Photochromism; Molybdenum; Intervalence charge transfer

1. Introduction

A powerful synthetic approach for the design of interpenetrated new organic–inorganic hybrid materials is the use of the synergistic interactions between the organic and inorganic components. In this context, the synthesis of new hybrid compounds based on polyoxometalates (POMs) has been found to be very versatile because of their structural and composition diversity.

POMs are inorganic oxide clusters of early transition metals (i.e. Mo, W, V, Ta, Nb). Because of their large variety of properties including molecular composition, size, morphologies, charge density, redox potential, photochemical response and acidity, molecular materials based on these polyanions are implicate in numerous disciplines such as catalysis [1], medicine [2] or material sciences [3].

Several strategies have been developed to this day to obtain hybrid organic–inorganic material based on POMs. For example, the functionalization of POMs with organic species to modify the chemical characters of the cluster surface has been largely explored in recent years. Most research works concern the substitution of terminal oxo-ligand by covalently bonded organic or organometallic groups [4]. Due to the low density of the surface charge associated to the π M–O interaction, favoring the polarization of the electronic cloud of the anion towards the interior of the cluster, the terminal M=O bonds on

*Corresponding author. Fax: +33 2 40 37 39 95.
E-mail address: stephane.jobic@cnrs-imn.fr (S. Jobic).

0022-4596/$ - see front matter © 2006 Elsevier Inc. All rights reserved.
doi:10.1016/j.jssc.2006.07.031

POMs are generally inert and their functionalities are often difficult. Another strategy consists to substitute the small cations associated with the POMs (H^+, Na^+, K^+, NH_4^+) by cationic organic molecules. POMs is then used as elementary building-blocks connected to organic parts via van der Waals, hydrogen bonding and/or electrostatic interactions, to obtain original hybrid frameworks with tunable dimensionality. The organic counterpart then acts not only as charge-compensating cations and template, but often plays a key role in the polymerization of the mineral component, and directs the crystallization of the supramolecular assemblies [5]. Moreover, the organic part may also stimulate fascinating physical behaviors which depend on the organic–mineral interface. For instance, it is speculated that photochromism in organic–inorganic hybrid compounds based on POMs originates from the ability of a labile hydrogen of the organic component to migrate towards the mineral component under UV–visible excitation [6]. Recently, in the course of new organic–inorganic hybrid materials with optical properties, we have embarked on the synthesis of new photochromic matrices obtained by self assembly of POMs associated with a large range of organoammonium counterions. Only the results with $HDBU^+$ cations are reported in this paper which is organized as followed. The synthesis and the structural and physical characterization of two new hybrid compounds $(HDBU)_3(NH_4)[\beta\text{-}Mo_8O_{26}]\cdot H_2O$ **1** and $(HDBU)_4[\delta\text{-}Mo_8O_{26}]$ **2** are reported in Section 2. In Section 3 the structure types of both compounds are described as well as the thermal and chemical isomerizations of the two $[Mo_8O_{26}]^{4-}$ isomers, and the optical properties of the materials. Finally, essential findings of our work are summarized in Section 4.

2. Experimental section

2.1. Materials and methods

1,8-diazabicyclo[5.4.0]undec-7-ene 98% $N_2C_9H_{17}$ (DBU), NH_4Cl, MoO_3 and $(NH_4)_6[Mo_7O_{24}]\cdot 4H_2O$ were purchased from Aldrich. All reagents were used without further purification. Hydrothermal syntheses have been carried out using 30 ml Teflon-lined autoclaves.

2.2. Synthesis of $(HDBU)_3(NH_4)[\beta\text{-}Mo_8O_{26}]\cdot H_2O$ 1

Method 1: $(NH_4)_6[Mo_7O_{24}]\cdot 4H_2O$ (1.235 g, 1 mmol) was dissolved in 15 ml of water. After addition of DBU (0.913 g, 6 mmol), pH was adjusted with HCl 1 M until 5.7. The mixture was stirred at room temperature for a few minutes and filtered to isolate a pure white solid of **1**. The powder was washed with H_2O, EtOH, Et_2O and dried in air (yield: 75%). Colorless needles of **1** suitable for X-ray structure analysis were obtained hydrothermally from white powder of **1** (160 °C, 24 h, autogenous pressure). *Anal*. Calcd for $C_{27}H_{57}O_{27}N_7Mo_8$: C, 19.31; H, 3.42; N, 5.83; Mo, 45.70. Found: C, 19.50; H, 3.38; N, 5.79; Mo, 44.77. FT-IR (cm^{-1}): $HDBU^+$ cations, 1645 (vs), 1586 (s), 1468 (m), 1440 (s), 1384 (w), 1355 (w), 1324 (s), 1293 (sh), 1207 (m), 1105 (m), 981 (w), 954 (w); NH_4^+ cations, 1400 (s), ν(Mo=O), 939 (vs), 910 (vs); ν(Mo–O–Mo), 842 (s) 720 (s), 669 (s), 628 (w), 557 (m), 524 (m), 473 (w), 452 (w). Thermal analysis reveals that compound **1** starts to decompose above 100 °C.

Method 2: Compound **1** has been obtained hydrothermally from a mixture of MoO_3 (0.720 g, 5 mmol), NH_4Cl (0.125 g, 1.27 mmol) and DBU (0.380 g, 2.5 mmol) in 20 ml of water (160 °C, 24 h, autogenous pressure). Large colorless needles were collected by filtration, washed with H_2O, EtOH, Et_2O and dried in air at room temperature (yield: 85%).

2.3. Synthesis of $(HDBU)_4[\delta\text{-}Mo_8O_{26}]$ 2

Method 1: $(NH_4)_6[Mo_7O_{24}]\cdot 4H_2O$ (1.235 g, 1 mmol) was dissolved in 15 ml of water. After addition of DBU (0.913 g, 6 mmol), pH was adjusted with HCl 1 M until 5.7 leading to the formation of a white solid of **1**. The mixture was then stirred at room temperature for few minutes and sealed in a 30 ml Teflon-lined autoclave (110 °C, 24 h, autogenous pressure). The resulting pale yellow blocks of 2 were filtered off, washed with H_2O, EtOH, Et_2O and dried in air at room temperature (yield: 85%). *Anal*. Calcd for $C_{36}H_{68}O_{26}N_8Mo_8$: C, 24.07; H, 3.81; N, 6.24; Mo, 42.72. Found: C, 24.22; H, 3.78; N, 6.26; Mo, 41.57. FT-IR (cm^{-1}): $HDBU^+$ cations, 1645 (vs), 1583 (s), 1468 (m), 1445 (m), 1392 (w), 1363 (w), 1325 (s), 1297 (w), 1207 (m), 1103 (m), 983 (w), 954 (w); ν(Mo=O), 954 (s), 927 (vs), 914 (vs); ν(Mo–O–Mo), 864 (vs), 815 (vs), 790 (vs), 723 (m), 690 (m), 650 (s), 536 (m). Thermal analysis reveals that compound **2** starts to decompose above 290 °C.

Method 2: Compound **2** has been obtained hydrothermally from a mixture of MoO_3 (0.720 g, 5 mmol) and DBU (0.380 g, 2.5 mmol) in 20 ml of water (160 °C, 24 h, autogenous pressure). Pale yellow crystals were collected by filtration, washed with H_2O, EtOH, Et_2O and dried in air at room temperature (yield: 85%).

2.4. Characterization and physical measurements

Elemental analyses of the solids were performed by the "Service d'Analyse du CNRS", in Vernaison (France). Thermogravimetric (DSC-TGA) data were measured by flowing dry nitrogen with a heating and cooling rate of 10 °C/min on a SETARAM TG-DSC 111 between 20 and 800 °C.

FT-IR spectra were recorded in the 4000–200 cm^{-1} range on a BRUKER Vertex equipped with an attenuated total reflection (ATR) device from Specac Eurolabo and computer control using the OPUS software.

Room temperature UV–vis diffuse reflectivity spectra were collected on a finely ground sample with a Cary 5G spectrometer (Varian). This instrument was equipped with a 60 mm diameter integrating sphere and computer control

using the "Scan" software. The reflectance versus wavelength measurements were made in the 250–800 nm range with a 2 nm step using Halon powder (from Varian) as reference (100% reflectance). The absorption (α/S) data were calculated from the reflectivity using the Kubelka–Munk function: $\alpha/S = (1-R)^2/2R$ where R is the reflectivity at a given wavelength, α is the absorption coefficient, and S is the scattering coefficient. The latter was supposed to be particle size independent, as expected for particles with diameter larger than few micrometers. The band gap was determined as the intersection point between the energy axis at the absorption offset and the line extrapolated from the linear portion of the absorption edge in the α/S versus E(eV) plot. The color evolution under illumination was followed by collecting diffuse reflectance spectra after different irradiation durations (from 10 min to the color saturation) under a UV lamp ($\lambda_{exc} = 365$ nm; $P = 12$ W, Fisher Bioblock labosi).

2.5. Structural characterizations

Crystals of **1** and **2** were glued at the tip of Lindemann capillaries by means of solvent free glue. Data collections were carried out at room temperature for **1** and −173 °C for **2** on a Bruker–Nonius Kappa CCD diffractometer, using graphite monochromatized MoK-$L_{2,3}$ radiation. The low temperature of the latter data collection was achieved by means of an Oxford cryostream cooler. Intensity integrations and standard Lorentz-polarization corrections were performed with the Bruker–Nonius Eval CCD program package. Subsequent calculations were conducted with the Jana2000 program suite [7], except for the crystal shape and dimension optimization which were performed with X-shape [8], based on the Habitus program [9], the direct methods which were carried out with Sir2004 [10] and the structure drawings which were realized with the Diamond program [11].

Starting from the model obtained through the application of the direct methods (basically the Mo and O atoms), the atomic positions of all atoms except hydrogen atoms could be easily found for both structures in the difference Fourier syntheses. Using anisotropic atomic displacement parameters, adding H atoms at calculated positions with riding parameters and introducing a secondary extinction coefficient [12], the refinements smoothly converged. For compound **1**, the refinement of the structure leads to a residual factor $R = 0.0697$ ($R_w = 0.0930$) for 10,234 independent observed reflections [$I/\sigma(I) \geqslant 2$] and 623 parameters and at $R = 0.163$ ($R_w = 0.124$) for all 20,970 independent reflections. For compound **2**, the refinement of the structure leads to a residual factor $R = 0.0226$ for 11,812 independent observed reflections [$I/\sigma(I) \geqslant 2$] and 354 parameters and at $R = 0.0339$ ($R_w = 0.0702$) for all 13,873 independent reflections. Crystal characteristics, data collection and reduction parameters, and refinement results are gathered in Table 1. Atomic parameters are reported in Table 2. Crystallographic data (excluding structure factors) for the structures reported in this paper have been deposited with the Cambridge Crystallographic Data Centre as supplementary publication no. CCDC 604573 & 604574. Copies of the data can be obtained free of charge on application to CCDC, 12 Union Road, Cambridge CB2 1EZ, UK (fax: (44) 1223 336-033; e-mail: deposit@ccdc.cam.ac.uk).

3. Results and discussion

3.1. Single-crystal X-ray analyses of $(HDBU)_3(NH_4)[\beta\text{-}Mo_8O_{26}]\cdot H_2O$ 1

The structure consists of two crystallographically independent $[Mo_8O_{26}]^{4-}$ anions, $HDBU^+$, NH_4^+ cations, and water molecules, linked together via hydrogen interactions. As shown in Fig. 1, the well-documented β-$[Mo_8O_{26}]^{4-}$ cluster, that is composed of two centro symmetrical $[Mo_4O_{13}]$ subunits, has the approximate C_{2h} symmetry and exhibits eight distorded edge-sharing $[MoO_6]$ octahedra. The oxygen sites fall broadly into four categories, terminal (O_t: O_2, O_3, O_7, O_8, O_{11}, O_{12}, O_{13}, O_{14}, O_{15}, O_{20}, O_{21}, O_{24}, O_{25}, O_{26}), twofold coordinated (μ_2-O: O_1, O_4, O_5, O_{16}, O_{17}, O_{18}), threefold coordinated (μ_3-O: O_9, O_{10}, O_{22}, O_{23}) and fivefold coordinated (μ_5-O: O_6, O_{19}). Each $[MoO_6]$ has three kinds of Mo–O bonds: two short (1.681(3)–1.746(3) Å), two medium (1.877(3)–1.991(3) Å) and two long (2.116(2)–2.369(2) Å). All $[MoO_6]$ polyhedra have a cis di-oxo conformation, except the Mo_3 and Mo_7 polyhedra which have only one Mo–O_t bond. Nevertheless, the Mo_7–O_{17} and Mo_3–O_5 distances are more typical of terminal oxygen bond length (1.734(3) and 1.746(3) Å, respectively) and these two O_{17} and O_5 sites have been often classified as pseudoterminal oxygen atoms [13].

$HDBU^+$ and NH_4^+, acting as charge-compensating cations and space-filling structural subunits, are connected to the β-$[Mo_8O_{26}]^{4-}$ clusters by a complex network of hydrogen interactions. Eight terminal oxygen atoms of two adjacent $[Mo_8O_{26}]^{4-}$ clusters form a pseudo tetragonal environment around NH_4^+ cations with short N–O distances in the 2.867(12)–3.024(12) Å range (Fig. 2a and b). The structure can then be described as $^1_\infty[NH_4Mo_8O_{26}]^{3-}$ infinite chains along the $[01\bar{1}]$ direction (i.e. the vertical axis in Fig. 2a and b), well separated by $HDBU^+$ cations and water molecules. The O_W water molecules connect the chains in the (011) plane with one short O_W-(μ^2-O) and one longer O_W–O_t distance (2.801(5) and 2.983(7) Å, respectively). In addition, the $HDBU^+$ cations are connected to the $^2_\infty[(NH_4)(H_2O)Mo_8O_{26}]^{3-}$ planes, with three kinds of hydrogen interactions (see Table 3). Two $HDDU^+$ cations, located between the chains, are bonded to two O_t with short and long O–H bonds (2.028(6) and 2.368(6) Å, respectively). The third type of $HDBU^+$ cations is located between the $2/\infty[(NH_4)(H_2O)Mo_8O_{26}]^{3-}$ planes and links water molecules with O–H bond length of 2.193(11) Å (see Fig. 2c).

Table 1
Crystallographic data and structure refinement for **1** and **2**

	1	2
(a) *Physical, crystallographic, and analytical data*		
Formula	$C_{27}H_{57}Mo_8N_7O_{27}$	$C_{36}H_{68}Mo_8N_8O_{26}$
Crystal color	colorless	colorless
Molecular weight ($g\,mol^{-1}$)	1679.3	1796.4
Crystal system	triclinic	triclinic
Space group	$P\bar{1}$	$P\bar{1}$
Temperature (K)	293	100
Cell parameters:		
a (Å)	11.2492(9)	11.3158(9)
b (Å)	14.1907(10)	11.3773(8)
c (Å)	16.7498(10)	13.2884(17)
α (°)	80.993(4)	92.110(8)
β (°)	72.272(6)	112.127(9)
γ (°)	71.696(7)	117.581(7)
V (Å^3)	2412.5(3)	1357.4(3)
Z	2	1
Density (calc., g/cm^{-3})	2.3110	2.1969
Crystal description	thick needle	block
Crystal size (mm^3)	$\sim 0.3 \times 0.09 \times 0.07$	$\sim 0.2 \times 0.2 \times 0.12$
(b) *Data collection*		
Diffractometer	Bruker–Nonius Kappa CCD	Bruker–Nonius Kappa CCD
Monochromator	oriented graphite (002)	oriented graphite (002)
Radiation	MoK-L$_{2,3}$ ($\lambda = 0.71069$ Å)	MoK-L$_{2,3}$ ($\lambda = 0.71069$ Å)
Scan mode	ω (1.7° per frame)	φ & ω (2.0° per frame)
hkl range	$-18 \leqslant h \leqslant 17$	$-17 \leqslant h \leqslant 19$
	$-18 \leqslant k \leqslant 22$	$-19 \leqslant k \leqslant 11$
	$-26 \leqslant l \leqslant 25$	$-22 \leqslant l \leqslant 22$
$\sin(\theta)/\lambda$ range (Å^{-1})	0.124–0.811	0.123–0.856
(c) *Data reduction*		
Linear absorption coeff. (mm^{-1})	2.099	1.875
Absorption correction	analytical (Gaussian integration)	analytical (Gaussian integration)
T_{min}/T_{max}	0.582/0.887	0.653/0.825
Number of reflections	65,687	39,174
No. of independent refl.	20,970	13,873
Criterions for observed reflections	$I > 2\sigma(I)$	$I > 2\sigma(I)$
R_{int} (all)	0.0697	0.0290
Average redundancy	3.1	2.8
No. of observed refl.	10,234	11,812
(d) *Refinement*		
Refinement	F^2	F^2
F(000)	1629	884
No. of refl. used in the refinement	20,970	13,873
No. of observed refl.	10,234	11,812
No. of refined parameters	623	354
R^a (obs)/R^a (all)	0.0570/0.163	0.0226/0.0339
$R_w{}^a$ (obs)/$R_w{}^a$ (all)	0.0930/0.124	0.0626/0.0702
S (obs)/S (all)	1.19/1.10	1.16/1.12
Weighting scheme	$w = 1/\left(\sigma^2(\lvert F_o\rvert^2) + 0.0019\lvert F_o\rvert^2\right)$	$w = 1/\left(\sigma^2(\lvert F_o\rvert^2) + 0.0019\lvert F_o\rvert^2\right)$
Secondary extinction coeff.	0.78(4)	0.59(3)
Difference Fourier residues	$[-2.88, +2.96]$ e$^-$/Å^3	$[-1.77, +1.28]$ e$^-$/Å^3

[a] $R = \sum \lvert\lvert F_o\rvert - \lvert F_c\rvert\rvert / \sum \lvert F_o\rvert$,

$R_w = \left[\sum w\left(\lvert F_o\rvert^2 - \lvert F_c\rvert^2\right)^2 / \sum w\left(\lvert F_o\rvert^4\right)\right]^{1/2}$.

3.2. Single-crystal X-ray analyses of $(HDBU)_4[\delta\text{-}Mo_8O_{26}]$ **2**

Compound **2** consists of discrete centro symmetrical octamolybdate clusters δ-$[Mo_8O_{26}]^{4-}$ with $HDBU^+$ cations. As shown in Fig. 3a, the δ-$[Mo_8O_{26}]^{4-}$ cluster has an approximate C_{2h} symmetry and is constructed from four distorted $[MoO_6]$ octahedra (Mo_2, Mo_3) and four $[MoO_4]$ tetrahedra (Mo_1, Mo_4) through edge- and

Table 2
Fractional atomic coordinates, equivalent isotropic displacement parameters (Å^2) and s.u.'s for **1** and **2**

Atom	x	y	z	U_{eq}
1				
Mo_1	−0.18588(4)	0.25919(3)	0.00139(2)	0.02667(14)
Mo_2	0.12559(4)	0.15592(3)	−0.03264(2)	0.02320(14)
Mo_3	−0.08986(3)	0.02938(3)	0.103558(19)	0.01880(12)
Mo_4	0.21744(4)	−0.06990(3)	0.07049(2)	0.02459(14)
Mo_5	0.18789(4)	0.24035(3)	0.47856(2)	0.02999(15)
Mo_6	−0.12430(4)	0.34723(3)	0.52258(2)	0.02467(14)
Mo_7	0.08513(3)	0.48135(3)	0.393422(19)	0.01881(12)
Mo_8	−0.22297(4)	0.58176(3)	0.43520(2)	0.02511(14)
O_1	−0.2961(3)	0.1833(2)	−0.00843(18)	0.0301(12)
O_2	−0.1556(3)	0.3075(2)	−0.09968(19)	0.0378(13)
O_3	−0.2915(3)	0.3542(2)	0.0579(2)	0.0455(15)
O_4	−0.0242(3)	0.2514(2)	0.02195(18)	0.0295(12)
O_5	−0.1873(3)	0.1520(2)	0.11599(16)	0.0266(11)
O_6	−0.0432(2)	0.09395(20)	−0.03751(15)	0.0209(10)
O_7	0.1489(3)	0.2041(2)	−0.13378(18)	0.0344(13)
O_8	0.2423(3)	0.1765(2)	0.0011(2)	0.0390(14)
O_9	0.0745(3)	0.0560(2)	0.08875(16)	0.0217(11)
O_{10}	0.2030(3)	0.0137(2)	−0.05895(16)	0.0224(11)
O_{11}	−0.1135(3)	−0.0262(2)	0.20130(17)	0.0306(12)
O_{12}	0.3471(3)	−0.0298(3)	0.0623(2)	0.0432(15)
O_{13}	0.1846(3)	−0.1210(2)	0.17092(18)	0.0377(14)
O_{14}	0.2926(4)	0.1559(2)	0.4109(2)	0.0513(16)
O_{15}	0.1670(3)	0.1760(2)	0.5733(2)	0.0425(15)
O_{16}	0.0226(3)	0.2553(2)	0.46001(18)	0.0315(13)
O_{17}	0.1811(3)	0.3611(2)	0.37196(17)	0.0288(12)
O_{18}	0.2970(3)	0.3120(2)	0.49447(19)	0.0320(12)
O_{19}	0.0451(2)	0.40271(18)	0.53072(15)	0.0189(10)
O_{20}	−0.2445(3)	0.3313(2)	0.4894(2)	0.0377(14)
O_{21}	−0.1400(3)	0.2899(2)	0.62019(18)	0.0348(13)
O_{22}	−0.0810(3)	0.4569(2)	0.40718(16)	0.0228(11)
O_{23}	−0.2035(3)	0.4850(2)	0.55931(16)	0.0217(10)
O_{24}	−0.3549(3)	0.5445(3)	0.4423(2)	0.0429(15)
O_{25}	−0.1925(3)	0.6429(2)	0.33939(19)	0.0392(14)
O_{26}	0.1035(3)	0.5468(2)	0.29971(17)	0.0319(12)
N_1	0.2031(5)	0.3642(4)	0.1278(3)	0.075(3)
N_2	0.0008(4)	0.3595(3)	0.2122(3)	0.0413(18)
N_3	0.4084(4)	−0.0769(3)	0.2386(2)	0.0390(17)
N_4	0.4774(4)	−0.1060(3)	0.3582(3)	0.049(2)
N_5	0.5361(4)	0.4452(3)	0.3506(2)	0.048(2)
N_6	0.4522(4)	0.4793(4)	0.2369(3)	0.049(2)
C_1	0.1571(7)	0.4421(5)	0.0695(4)	0.079(4)
C_2	0.0330(8)	0.5101(6)	0.1112(6)	0.106(5)
C_3	−0.0654(7)	0.4515(5)	0.1659(5)	0.093(4)
C_4	0.1261(5)	0.3226(4)	0.1894(3)	0.035(2)
C_5	0.1883(5)	0.2326(4)	0.2323(4)	0.057(3)
C_6	0.1568(5)	0.1413(4)	0.2287(3)	0.046(2)
C_7	0.0266(6)	0.1354(5)	0.2775(4)	0.061(3)
C_8	−0.0803(7)	0.2168(5)	0.2582(3)	0.066(3)
C_9	−0.0824(5)	0.3134(4)	0.2771(4)	0.054(3)
C_{10}	0.5178(6)	−0.0414(5)	0.1881(4)	0.064(3)
C_{11}	0.5586(6)	0.0057(6)	0.2437(4)	0.076(4)
C_{12}	0.5880(6)	−0.0653(7)	0.3143(5)	0.095(4)
C_{13}	0.3912(5)	−0.1037(3)	0.3188(3)	0.0346(19)
C_{14}	0.2717(5)	−0.1296(4)	0.3641(3)	0.049(2)
C_{15}	0.1855(6)	−0.0598(5)	0.4332(4)	0.059(3)
C_{16}	0.2267(8)	−0.0820(5)	0.5136(4)	0.076(3)
C_{17}	0.3597(7)	−0.0768(4)	0.5073(4)	0.068(3)
C_{18}	0.4644(7)	−0.1452(5)	0.4450(4)	0.072(3)
C_{19}	0.5541(5)	0.3393(5)	0.3555(3)	0.054(3)
C_{20}	0.5736(6)	0.3096(4)	0.2688(3)	0.056(3)
C_{21}	0.4675(5)	0.3731(5)	0.2321(3)	0.058(3)
C_{22}	0.4869(5)	0.5084(4)	0.2954(3)	0.046(2)
C_{23}	0.4758(6)	0.6147(5)	0.2972(4)	0.068(3)
C_{24}	0.5680(7)	0.6523(5)	0.2221(5)	0.080(4)
C_{25}	0.5218(7)	0.6785(5)	0.1430(4)	0.080(4)
C_{26}	0.4966(6)	0.5968(5)	0.1124(4)	0.073(3)
C_{27}	0.3982(6)	0.5495(5)	0.1740(4)	0.069(3)
N_7	−0.0097(4)	0.7638(3)	0.2587(2)	0.0329(15)
O_w	0.4406(4)	0.2035(3)	0.0731(3)	0.069(2)
2				
Mo_1	0.519702(13)	0.361043(12)	0.248992(10)	0.00903(5)
Mo_2	0.815991(12)	0.606391(11)	0.488289(9)	0.00710(4)
Mo_3	0.203302(12)	0.258587(11)	0.300115(9)	0.00753(4)
Mo_4	0.488461(12)	0.634885(11)	0.428536(9)	0.00651(4)
O_1	0.60656(11)	0.61803(10)	0.37988(8)	0.0098(4)
O_2	0.67411(11)	0.42000(10)	0.39032(9)	0.0098(4)
O_3	0.34811(11)	0.34745(11)	0.24090(9)	0.0115(4)
O_4	0.57515(13)	0.46048(13)	0.16469(10)	0.0165(5)
O_5	0.47753(13)	0.20131(12)	0.19370(10)	0.0178(5)
O_6	0.93655(12)	0.57086(11)	0.58325(9)	0.0127(4)
O_7	0.89882(12)	0.68097(11)	0.40646(9)	0.0125(4)
O_8	0.85619(11)	0.76780(10)	0.58035(8)	0.0091(4)
O_9	0.12899(13)	0.09057(11)	0.23975(10)	0.0156(4)
O_{10}	0.08148(12)	0.30038(12)	0.21482(9)	0.0142(4)
O_{11}	0.34157(11)	0.46848(10)	0.42406(9)	0.0094(4)
O_{12}	0.40614(12)	0.71297(11)	0.34479(9)	0.0133(4)
O_{13}	0.59604(11)	0.74076(10)	0.56681(9)	0.0099(4)
N_1	0.80981(14)	0.98308(13)	0.48758(10)	0.0119(5)
N_2	0.77000(14)	1.09733(12)	0.35061(10)	0.0107(5)
N_3	0.17990(14)	0.76083(13)	0.20527(11)	0.0142(5)
N_4	−0.05462(14)	0.71443(13)	0.08635(10)	0.0112(5)
C_1	0.78438(18)	1.05641(15)	0.56141(13)	0.0152(6)
C_2	0.67646(18)	1.09707(17)	0.48921(14)	0.0166(6)
C_3	0.73467(17)	1.17592(16)	0.41319(13)	0.0146(6)
C_4	0.80124(15)	1.00517(13)	0.38857(11)	0.0097(5)
C_5	0.82263(17)	0.91746(15)	0.31932(13)	0.0134(6)
C_6	0.68400(19)	0.82817(16)	0.20818(13)	0.0180(6)
C_7	0.67143(19)	0.90368(18)	0.11562(14)	0.0209(7)
C_8	0.65066(18)	1.02285(18)	0.13981(13)	0.0186(6)
C_9	0.77525(17)	1.13336(16)	0.24662(13)	0.0140(6)
C_{10}	0.25534(17)	0.89307(16)	0.18146(13)	0.0161(6)
C_{11}	0.16047(19)	0.88873(16)	0.06349(13)	0.0171(6)
C_{12}	0.00344(17)	0.83789(14)	0.04601(12)	0.0138(6)
C_{13}	0.03353(16)	0.68111(15)	0.15976(12)	0.0112(5)
C_{14}	−0.02965(19)	0.54971(16)	0.19277(13)	0.0159(6)
C_{15}	−0.11283(17)	0.42196(16)	0.09557(13)	0.0145(6)
C_{16}	−0.26908(17)	0.38383(16)	0.01342(14)	0.0168(6)
C_{17}	−0.27970(17)	0.49388(16)	−0.04546(14)	0.0181(6)
C_{18}	−0.21790(17)	0.62709(16)	0.03752(14)	0.0166(6)

corner-sharing. It can be described as a central Mo_6O_6 ring composed by two pairs of edge-sharing octahedra connected by two tetrahedra via μ_2-O atoms (O_3 and O_2). The ring is then capped on opposite faces by two tripodal corner-sharing tetrahedra (Fig. 3b). The distorted [MoO_6] octahedra have two Mo–O_t short bonds (O_6, O_7, O_9, O_{10}) in the 1.6936(13)–1.7015(12) Å range, three Mo–O(μ_2) bonds (O_1, O_2, O_8) (1.9281(12)–2.3328(12) Å) and one Mo–O(μ_3) bond (O_{11}) (2.2743(9)–2.3435(13) Å). The [MoO_4] tetrahedra of the ring have two short Mo–O_t

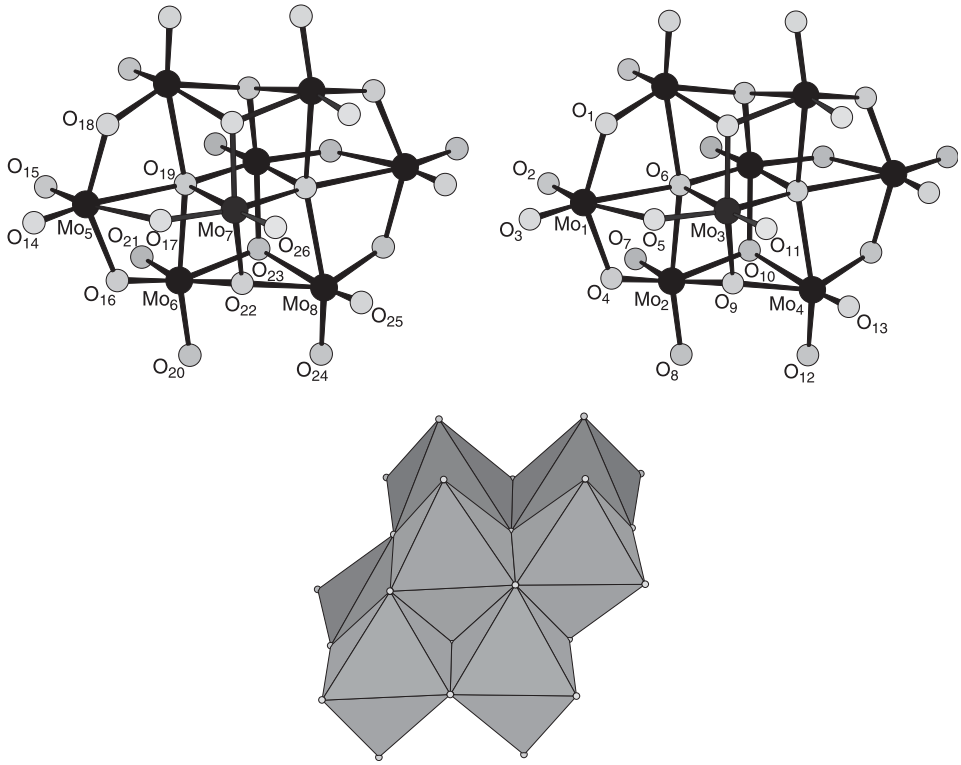

Fig. 1. Ball and stick representation of the two β-$[Mo_8O_{26}]^{4-}$ anions in compound **1** showing the labelling scheme (top) and schematic polyhedral representation of the β-$[Mo_8O_{26}]^{4-}$ building block in **1** (down).

bonds (O_4, O_5) (1.7012(14) and 1.7043(15) Å) and two slightly longer Mo–O(μ_2) bonds (O_2, O_3) (1.8355(14) and 1.8385(9) Å). The capping $[MoO_4]$ tetrahedra have three kinds of Mo–O bond: one short Mo–O_t bond (1.7186(14) Å), two Mo–O(μ_2) bonds (1.7616(9) and 1.7663(15) Å) and one Mo–O(μ_3) bond (1.8314(10) Å).

Each δ-$[Mo_8O_{26}]^{4-}$ anion is linked through short hydrogen bonds to four $HDBU^+$ cations (see Table 3), two are connected to the terminal oxygen atoms (O_{12}) of the capping $[MoO_4]$ tetrahedra and two others are linked to the μ_2-O atom (O_8) of the edge-sharing octahedral dimers with O–H bond distances of 1.941 and 2.068 Å, respectively, as shown in Fig. 4.

3.3. Synthesis

The addition of DBU to an aqueous solution of ammonium heptamolybdate at pH 5.7 has led to the formation of two new organic–inorganic hybrid compounds containing two different $[Mo_8O_{26}]^{4-}$ clusters. Compound **1** is obtained at room temperature in high yield as Eq. (1), while compound **2** is formed quantitatively by hydrothermal condition from **1** at 110 °C as Eq. (2).

$$8[Mo_7O_{24}]^{6-} + 21DBU + 7NH_4^+ + 41H_3O^+ \leftrightarrows 7(HDBU)_3(NH_4)[\beta\text{-}MO_8O_{26}]\cdot H_2O + 51H_2O \quad (1)$$

$$(HDBU)_3(NH_4)[\beta\text{-}MO_8O_{26}]\cdot H_2O + HDBU^+ \leftrightarrows (HDBU)_4[\delta\text{-}MO_8O_{26}] + NH_4^+ + H_2O \quad (2)$$

In the past two decades, nine isomers of the $[Mo_8O_{26}]^{4-}$ cluster namely α [14,15], β [16–18], γ [19,20], δ [21–24], ε [25], ζ [26,27], ξ [28], η [29] and θ [30,31] have been discovered and characterized in the solid state by conventional crystallization or by hydrothermal conditions. Their topology has been well described [32] and differs by the number and the connectivity of the different types of Mo polyhedra, as summed up in Table 4. While the β-$[Mo_8O_{26}]^{4-}$ cluster is commonly observed in numerous organic–inorganic hybrid compounds, associated with a large variety of ammonium cations (see for example [33–38]), the δ-isomer has only previously been described for very few compounds principally using hydrothermal conditions. Those conditions constitute a well-appropriated route to synthesize metastable organic–inorganic hybrid phases, allowing the introduction of organic components into oxide matrices [5,39].

The thermal and chemical interconversion pathways of both compounds **1** and **2** have been highlighted and can be deconvoluated as displayed in Scheme 1.

Step 1: At room temperature and pH = 5.7, the $[Mo_7O_{24}]^{6-}$ anion is rapidly converted to the more acidic β-$[Mo_8O_{26}]^{4-}$ polyoxometalate [40] that precipitates instantaneously with $HDBU^+$ and NH_4^+ cations to form compound **1**.

Step 2: Using hydrothermal conditions at 110 °C, the slurry of **1** in the mother liquor is quantitatively converted to **2** via a dissolution-crystal growth process. This process includes an intramolecular isomerization in solution from

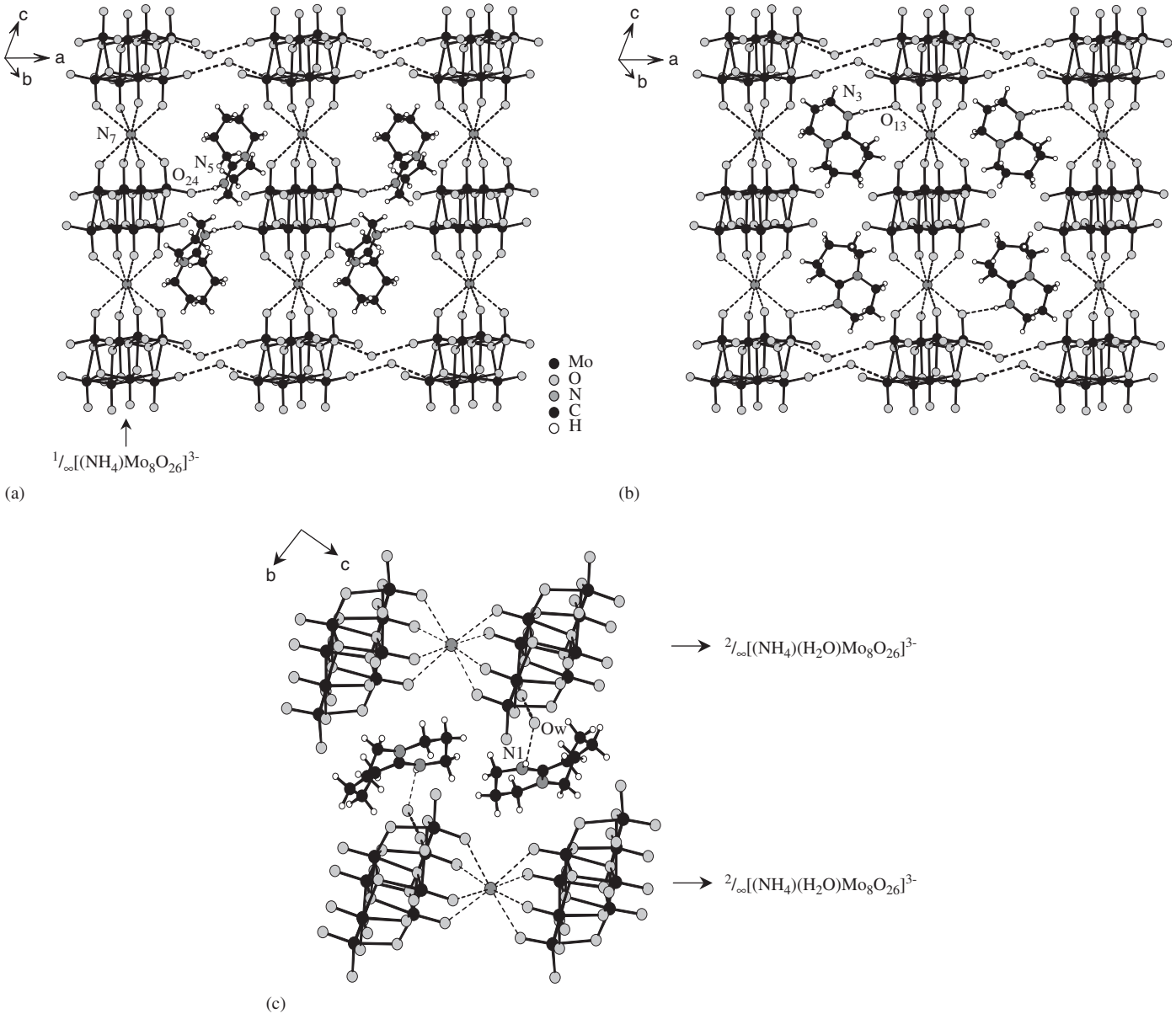

Fig. 2. Assembly of β-$[Mo_8O_{26}]^{4-}$ blocks into $^1_\infty[(NH_4)Mo_8O_{26}]^{3-}$ infinite chains (a and b). Chains connect to each other to form $^2_\infty[(NH_4)(H_2O)Mo_8O_{26}]^{3-}$ layers via water molecules. $HDBU^+$ cations are linked to the mineral network via three types of hydrogen bonds (a, b and c).

Table 3
Hydrogen bonding geometry (Å, °)

N–H···O	N–H	H···O	N···O	N–H···O
1				
N_5–H_3···O_{24}	0.95	2.03	2.959(6)	166.17
N_3–H_2···O_{13}	0.95	2.36	3.311(6)	172.43
N_1–H_1···O_w	0.95	2.19	2.918(6)	132.25
2				
N_1–H_1···O_8	0.92	2.06	2.953(2)	160.97
N_3–H_2···O_{12}	0.97	1.94	2.842(2)	153.50

the β-$[Mo_8O_{26}]^{4-}$ to the δ-$[Mo_8O_{26}]^{4-}$ cluster and the concomitant substitution in the solid state of one NH_4^+ by one $HDBU^+$ cation per inorganic discrete block. In solution, chemical isomerization between $[Mo_8O_{26}]^{4-}$ isomers has already been reported. For instance, the dynamic stereochemistry of the α-isomer has been shown by a ^{17}O-NMR solution study [41] and the $\alpha \leftrightarrows \beta$ interconversion has been characterized in the acetonitrile solution by IR spectroscopy [42]. This unexpected isomerization of the two structurally disparate isomers has been explained via a "bond-breaking/making" mechanism based on an intramolecular rearrangement of the Mo–O bonds and the formation, as a suspected intermediate species, of a third γ-$[Mo_8O_{26}]^{4-}$ isomer that contains two molybdenum atoms in a square pyramidal environment. This mechanism has been reinforced by the characterization in the solid state of the γ-isomer few years later [43]. To some extent, the δ-isomer may be viewed as a derivative form of the α

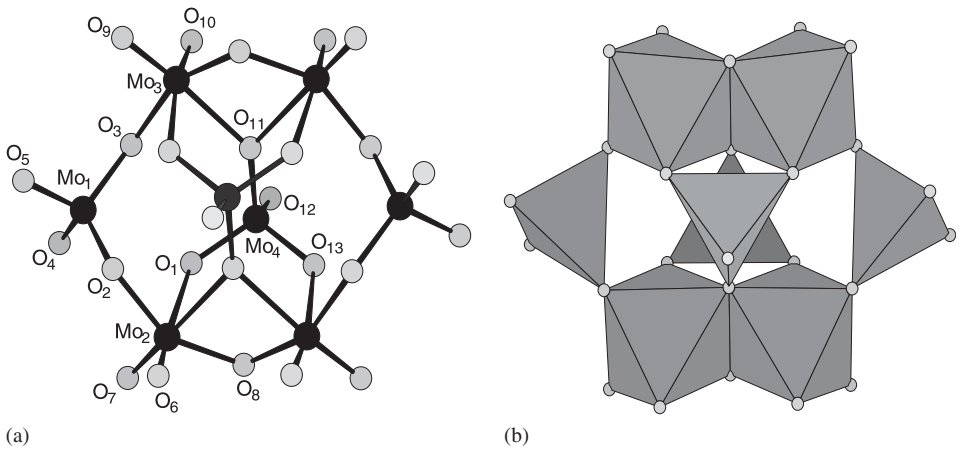

Fig. 3. Ball and stick representation of the δ-$[Mo_8O_{26}]^{4-}$ anions in compound **2** showing the labelling scheme (a). Schematic polyhedral representation of the δ-$[Mo_8O_{26}]^{4-}$ isomer (b).

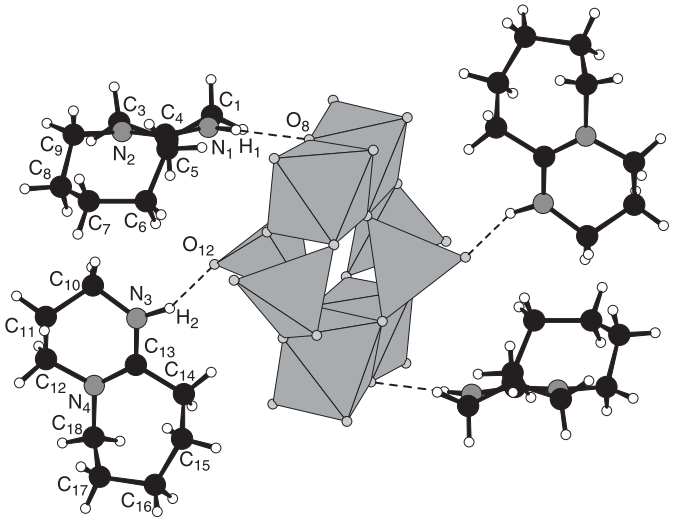

Fig. 4. Representation of the chemical environment of the δ-$[Mo_8O_{26}]^{4-}$ anion in **2** where hydrogen bonds are highlighted.

one where two trans molybdenum cations leave their sixfold coordination to give rise to $[MoO_4]$ tetrahedra. Formally, in the δ-isomer of **2**, the Mo_1–O_1 and Mo_1–O_{13} distances (2.8664(12) and 3.204(11) Å, respectively) are too long to be considered as two Mo–O bonds. At the opposite, in the α-isomer these two contacts are shortened up to about 2.4 Å and all Mo atoms of the ring are then sixfold coordinated.

As reported in the literature, the $\alpha \leftrightarrows \beta$ isomerization depends on the nature of counter-cations. The β-isomer, that has the most compact structure among the nine isomers, is more stabilized with small cations (Na^+, K^+, NH_4^+ [44,45]), while the addition of large cations such as NBu_4^+ [46], or $[(C_3H_7)(C_6H_5)_3P]^+$ [42] to an acidified aqueous solution (pH 3–4) of sodium molybdate leads to the formation of the α-isomer in the solid state. Consequently, during the interconversion of **1** into **2** at 110 °C, the $\beta \leftrightarrows \gamma \leftrightarrows \alpha$ isomerization in solution may occur. In a second step, the conversion of α-$[Mo_8O_{26}]^{4-}$ in solution to δ-$[Mo_8O_{26}]^{4-}$ in the solid state may be attributed to stress effects occurred during the crystallization with $HDBU^+$ cations. As described in the experimental part, the formation of **2** at 110 °C requests an excess of DBU (nDBU/$n[Mo_7O_{24}]^{6-} = 6$) since a similar reaction in stoechiometric amount, as reported in Eq. (2) (i.e. nDBU/$n[Mo_7O_{24}]^{6-} = 3.5$), leads to a mixture of **1** and **2**.

Step 3: The thermal interconversion from **2** to **1** in hydrothermal conditions for temperatures beyond 110 °C has been characterized by a series of experiments. DBU was added to an aqueous solution of ammonium heptamolybdate ([Mo] = 0.35 M). After adjusting the pH until 5.7 by HCl 1 M, the slurry of **1** in the mother liquor were then placed into a 30 ml Teflon-lined autoclave and were stood for 24 h at different temperatures: 110, 130, 160 and 180 °C. In each case, the final products were characterized by FT-IR spectroscopy and powder X-ray diffraction analyses (by comparison of the experimental X-ray diffraction patterns with the simulated ones obtained from single-crystal X-ray diffraction files of **1** and **2**). At 110 °C, a pure phase of **2** is observed, clearly showing the quantitative interconversion from **1** to **2**. In the 110–160 °C range, the final products are a mixture of both compounds in which **1** is the majority species at 130 °C and the minority species at 160 °C. At 180 °C, a pure phase of **1** has been characterized, showing that the quantitative interconversion from **2** to **1** is achieved and seems to proceed via a $[Mo_8O_{26}]^{4-}$ isomerization mechanism similar to the one described in step 2.

The interconversion of the β-isomer to the δ-one is more dependant on the presence of NH_4^+ cations in solution than on the temperature value. Many experiments have been realized, using MoO_3 as a starting material, to obtain ammonium cation exempt media. Compound **2** has been synthesized hydrothermally by stoechiometric addition of DBU to a MoO_3 slurry in aqueous solution, following Eq. (3). A series of experiments has been realized at different temperatures: 110, 130, 160 and 180 °C. In each case, the final products were characterized by powder

Table 4
Summary of selected structural characteristics of $[Mo_8O_{26}]^{4-}$ isomers

	octahedra	tetrahedra	square pyramid	O_t	$O(\mu_2)$	$O(\mu_3)$	$O(\mu_4)$	$O(\mu_5)$
α	6	2	—	14	6	6	—	—
β	8	—	—	14	6	4	—	2
γ	6	—	2	14	6	4	2	—
δ	4	4	—	14	10	2	—	—
ε	2	—	6	14	4	6	—	—
ζ	4	—	4	14	6	6	—	—
ξ	4	—	4	14	6	6	—	—
η	6	—	2	14	4	8	—	—
θ	4	2	2	14	8	4	—	—

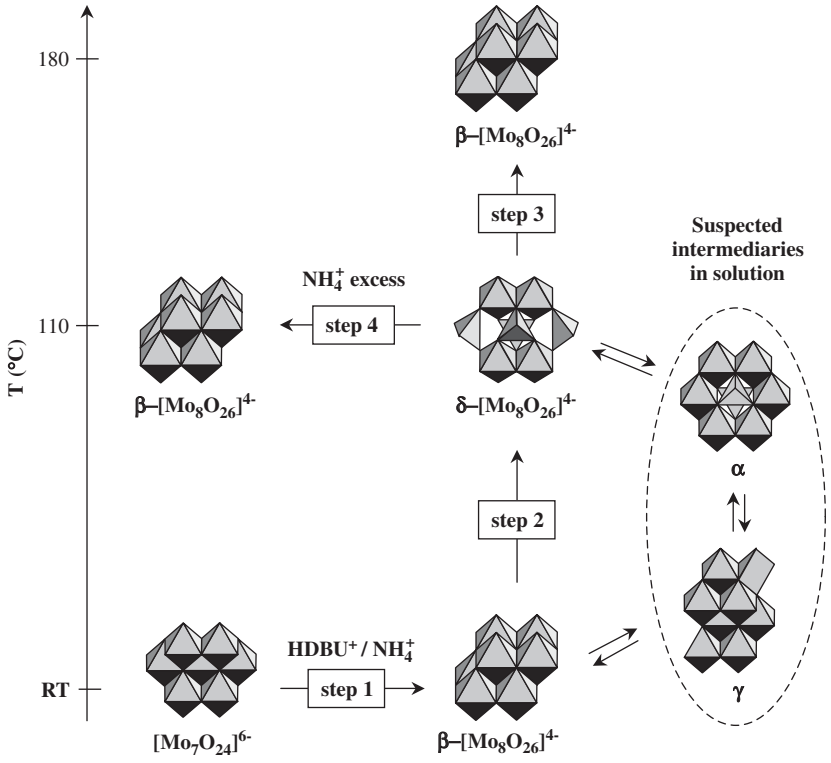

Scheme 1.

X-ray diffraction analyses (see supplementary materials). For temperatures ranging from 110 to 130 °C, X-ray diffraction patterns have shown a mixture of **2** and the initial MoO_3, while pure phase of **2** has been obtained in the 160–180 °C temperature range. In contrast, similar reactions carried out at 160 and 180 °C in presence of NH_4^+ cations have led to pure compound **1**, following Eq. (4). Thus, to sum up, if ammonium heptamolybdate is used as starting material, compound **2** is isolated as a pure phase at 110 °C and the conversion from **2** to **1** is progressively observed with increasing the temperature. In contrast, compound **2** obtained from MoO_3 is stable at temperature beyond 110 °C and the interconversion takes place only if NH_4^+ cations are introduced in the media.

$$8MoO_3 + 4DBU + 2H_2O \rightarrow (HDBU)_4[\delta\text{-}MO_8O_{26}] \quad (3)$$

$$8MoO_3 + 4DBU + 3H_2O + NH_4{}^+ \rightarrow (HDBU)_3(NH_4)[\beta\text{-}MO_8O_{26}] \cdot H_2O + HDBU^+ \quad (4)$$

Step 4: At 110 °C, the δ-$[Mo_8O_{26}]^{4-}$ anion is stabilized in the solid state but, according to Eq. (2), chemical interconversion from **2** to **1** at this temperature should be triggered by the introduction of an excess of NH_4^+ cations in the solution. An excess of NH_4Cl was therefore added to a mixture of compound **2** in H_2O to obtain a NH_4^+/Mo ratio = 2.5 and the slurry was sealed in a 30 ml Teflon-lined autoclaves and kept at temperature of 110 °C for 3 days. Large colorless crystals of compound **1** (yield in crystal

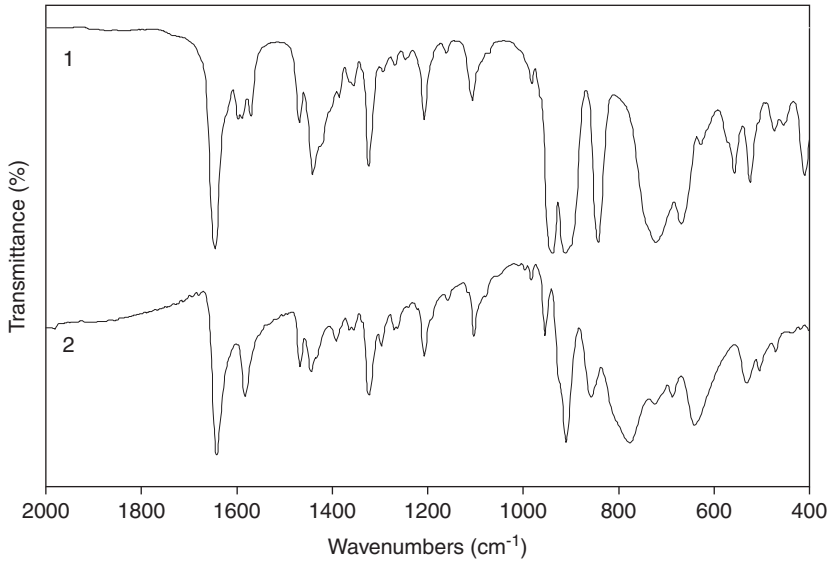

Fig. 5. IR spectra of **1** and **2** between 2000 and 400 cm^{-1}.

65%) were then isolated and characterized by X-ray diffraction pattern checking the aforementioned prediction.

3.4. Optical properties

3.4.1. FT-IR spectroscopy

In both IR-spectra of compounds **1** and **2** displayed in Fig. 5, the $HDBU^+$ cation absorption bands are located between 1645 and 1000 cm^{-1}. The spectrum of **1** shows in addition a strong absorption band at 1400 cm^{-1}, attributed to the N–H stretching vibrations mode of the NH_4^+ cations present in the network. Below 1000 cm^{-1}, the two spectra present some significant differences in the range corresponding to the Mo–O vibrations of the two $[Mo_8O_{26}]^{4-}$ isomers, that allows their unambiguous distinction. For compound **1**, the β-$[Mo_8O_{26}]^{4-}$ cluster is characterized by four strong absorption bands at 950, 939, 910 and 900 cm^{-1}, corresponding to the $Mo{=}O_t$ vibrations, and by three strong absorption bands at 842, 720 and 669 cm^{-1}, attributed to $\nu Mo–O_\mu$ vibrations [43]. The δ-$[Mo_8O_{26}]^{4-}$ isomer in compound **2** is characterized by only two strong absorption bands at 927 and 914 cm^{-1}, related to the $Mo{=}O_t$ vibrations, and two strong absorption bands located at 815 and 790 cm^{-1} and attributed to $\nu Mo–O_\mu$ vibrations [21].

3.4.2. Photochromism behavior

The diffuse reflectance spectra of **1** and **2** and their associated Kulbelka–Munk transforms are displayed in Fig. 6. The α/S energy spectra evidence a well-defined absorption threshold around 3.62 and 3.72 eV for **1** and **2**, respectively. The optical gap is associated to an intramolecular oxygen to molybdenum charge transfer (LMCT) which differs in energy (as expected) when going from the β-$[Mo_8O_{26}]^{4-}$ to the δ-$[Mo_8O_{26}]^{4-}$ building blocks. The

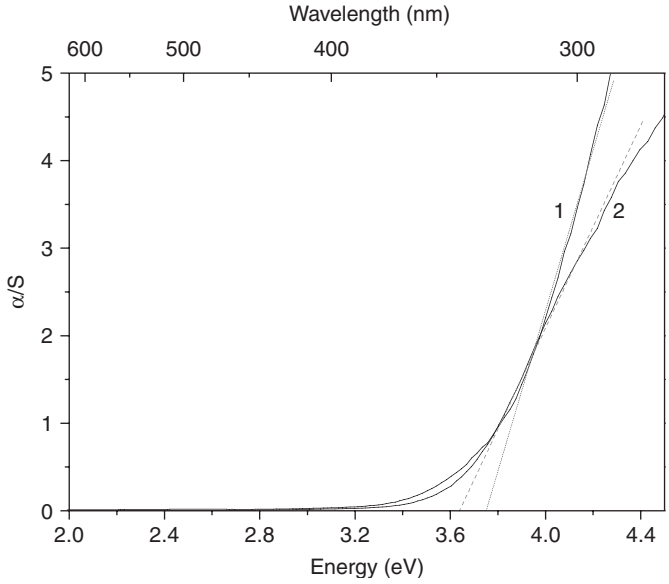

Fig. 6. Diffuse UV–vis reflectance after Kubelka–Munk transformation versus energy for **1** and **2**.

difference is due to a modification of the O-2p/Mo-4d orbital hybridization, in relation with structural changes (edge sharing $[MoO_6]$ polyhedra in β-blocks vs. edge and corner sharing $[MoO_6]$ polyhedra and $[MoO_4]$ tetrahedra in δ-blocks). The observed optical gaps agree well with the white color of the powdered samples. It is worth noticing that the yellow pale hue of single crystals of **2** disappears under grinding.

Figs. 7 and 8 account for the behavior of **1** and **2** under UV excitation. For both compounds, the LMCT onset moves slightly towards lower energy under UV excitation. Concomitantly, an absorption band, peaking at about 2.65

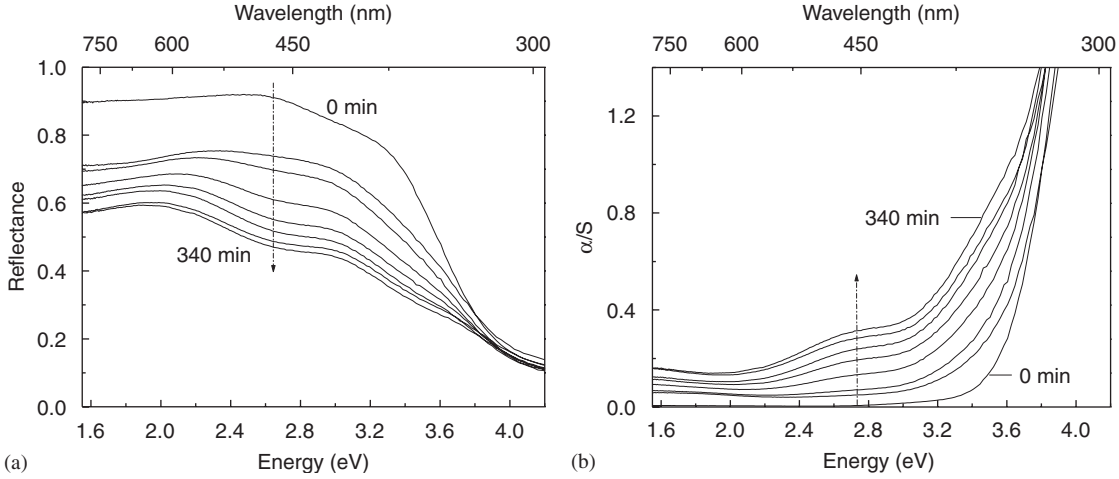

Fig. 7. Evolution of the reflectance (a) and the Kubelka–Munk transformation (b) of **1**, versus energy with irradiation duration at 365 nm (0′, 10′, 20′, 50′, 110′, 160′, 250′ and 340′). Color saturation is reached after 340′ excitation.

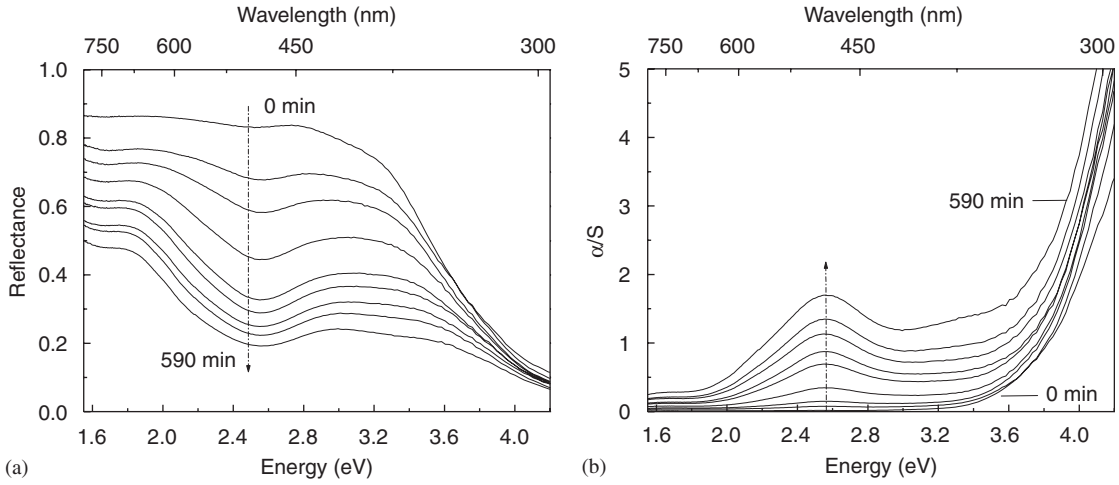

Fig. 8. Evolution of the reflectance (a) and the Kubelka–Munk transformation (b) of **2**, versus energy with irradiation duration at 365 nm (0′, 10′, 20′, 50′, 110′, 150′, 240′, 330′and 590′). Color saturation is reached after 590′ excitation.

and 2.55 eV for **1** and **2**, respectively, shows up, increases up to saturation, and broadens with exposure duration, while the base line between the two absorption regions is raised. The evolution with time of the diffuse reflectance spectra goes along with the successive colors observed for **1** and **2** under UV excitation, i.e. the sequences white → yellowish brown → light brown for **1**, and white → pale purple → yellowish brown → brown for **2**. At the time scale of the week, the photo-induced hues in **1** and **2** are irreversible at RT in darkness and daylight.

The appearance of the absorption bands peaking at 2.65 and 2.55 eV results from the reduction of Mo^{6+} into Mo^{5+} under UV excitation. The higher the concentration in Mo^{5+}, the higher the probability to observe on-site *d–d* electronic transitions and/or homonuclear intervalence charge transfers, the more intense the color change (stronger absorption). This change is unfortunately limited to the surface of the irradiated grains, due to the absorption of the impinging light in a relatively short distance.

The displacement in energy of the LMCT band may be related to the increase in Mo^{5+} concentration under illumination. Due to a lower covalence of the Mo^{5+}–O^{2-} bond compared with the Mo^{6+}–O^{2-} bond, the bottom of the Mo d-block should be stabilized in energy with Mo^{5+} concentration.

At this stage, the origin of the photochromism in organic–inorganic hybrid materials based on polyoxometalates may be explained in terms of the seminal Yamase's model [6]. Briefly, this model suggests that electrons of terminal anions (O_t), the strongest oxygen bonded to Mo via σ and π bonding interactions, are promoted towards the Mo^{6+}-d block under higher than optical gap UV–visible excitation. To annihilate the photo-generated hole, a labile proton of the organic component moves then towards a basic oxygen anion (e.g. μ_2-O or μ_3-O) while concomitantly an electron of the amino nitrogen atom is retroceded to the mineral framework to form a charge transfer complex with appearance of a weak nitrogen–oxygen bond. Nevertheless, this model has several shortcomings: (i) The photochromic

process is strongly dependent on the hydrogen bond subnetwork and, consequently, upon the spatial distribution of hydrogen atoms around the mineral component. Namely, the presence of N–H$\cdots\mu_2$-O or N–H$\cdots\mu_3$-O contacts are of prime importance to favor the stabilization of a metastable state under illumination with coexistence of Mo^{5+} and Mo^{6+} cations, even if this criterion is not sufficient to predict photochromism. However, during our investigation on hybrid Mo-POMs, photochromism has been observed in materials where hydrogen is only involved in hydrogen bond with terminal oxygen atoms (unpublished results) which rebuts the Yamase' model. (ii) To facilitate the electron retro-donation from the amino nitrogen atom towards one oxidized oxygen anion of the mineral counterpart, some orbital overlap between the two protagonists is expected. This implies the occurrence of short N$\cdots$O contacts and an appropriate orientation of the organic part with regards to the inorganic one. This criterion is not systematically observed. The model could be maintained though if an undetected structural rearrangement would take place at the surface of the material. (iii) So far, according to Yamase the color change occurs only if the incident light bears energy higher than the energy requested to get over the optical gap. Typically, **2** can shift from white to brown under excitation at 413 nm, that is 0.7 eV below its absorption threshold determined from Kulbelka–Munk transformed reflectance spectra. (iv) The Yamase' model suggests the occurrence of free radicals on the organic part in the colored state. So far, if those free radicals have been observed by EPR in Keggin anions containing hybrid materials [47], their existence in isopolyoxometalate has never been proved.

4. Conclusion

The syntheses of two new hybrid organic–inorganic compounds based on Mo-POMs and $HDBU^+$ cations, have been presented in this paper. $(HDBU)_3(NH_4)[\beta\text{-}Mo_8O_{26}]\cdot H_2O$ **1** and $(HDBU)_4[\delta\text{-}Mo_8O_{26}]$ **2** are obtained at room temperature or via hydrothermal syntheses by self-assembly of two $[Mo_8O_{26}]^{4-}$ isomers and organoammonium cations to form a 3D framework via hydrogen interactions. These compounds present both thermal and chemical isomerizations. The **1** to **2** interconversion occurs hydrothermally at 110 °C but **1** can be regenerate from **2** with increasing the temperature above 110 °C or by adding NH_4^+ cations. This isomerization between the β-isomer and the δ-isomer of the octamolybdate had never been pointed out yet, to our knowledge. Besides, optical properties of **1** and **2** have been reported. Both compounds show photochromic behavior under UV-irradiation. **1** goes from white to light brown, whereas **2** turns up brown via intermediate color stages. Moreover, even if the Yamase' model is widely adopted to explain the photochromic properties of organic–inorganic hybrid materials based on polyoxometalates, some shortcomings have been pointed out and some corrections should have to be applied in the future to better address the color change mechanism under UV–visible illumination in hybrid compounds.

Appendix A. Supplementary materials

Supplementary materials associated with this article can be found in the online version at doi:10.1016/j.jssc.2006.07.031.

References

[1] N. Mizuno, M. Misono, Chem. Rev. 98 (1998) 199–218.
[2] J.T. Rhule, C.L. Hill, D.A. Jude, R.F. Schinazi, Chem. Rev. 98 (1998) 327–358.
[3] D.E. Katsoulis, Chem. Rev. 98 (1998) 359–387.
[4] P. Gouzerh, A. Proust, Chem. Rev. 98 (1998) 77–111.
[5] P.J. Hagrman, D. Hagrman, J. Zubieta, Angew. Chem. Int. Ed. 38 (1999) 2638–2684.
[6] T. Yamase, Chem. Rev. 98 (1998) 307–326.
[7] V. Petricek, M. Dusek, JANA2000, a Crystallographic Computing System, Institute of Physics, Academy of Sciences of the Czech Republic, Prague, Czech Republic, 2000.
[8] Stoe & Cie. X-shape (version 1.02), Stoe & Cie, Darmstadt, Germany, 1996.
[9] W. Herrendorf, Habitus. Ph.D. dissertation, University of Karlsruhe, Germany, 1993.
[10] M.C. Burla, R. Caliandro, M. Camalli, B. Carrozzini, G.L. Cascarano, L. De Caro, C. Giacovazzo, G. Polidori, R. Spagna, SIR2004: an improved tool for crystal structure determination and refinement, J. Appl. Crystallogr. 38 (2005) 381–388.
[11] K. Brandenburg, Diamond version 3, Crystal Impact GbR, Bonn, Germany, 2001.
[12] P.J. Becker, P. Coppens, Acta Crystallogr. A 30 (1974) 129–147.
[13] A.J. Bridgeman, G. Cavigliasso, Inorg. Chem. 41 (2002) 3500–3507.
[14] D. Hagrman, P. Hagrman, J. Zubieta, Inorg. Chim. Acta 300–302 (2000) 212–224.
[15] G. Kalpana, K. Vidyasagar, Acta Crystallogr. E 61 (2005) m1885–m1886.
[16] C.-D. Wu, C.-Z. Lu, X. Lin, H.-H. Zhuang, J.-S. Huang, Inorg. Chem. Commun. 5 (2002) 664–666.
[17] C. Qin, X. Wang, Y. Qi, E. Wang, C. Hu, L. Xu, J. Solid. State. Chem. 177 (2004) 3263–3269.
[18] S. Lu, Y. Ke, J. Li, Y. Zhang, Solid State Sci. 5 (2003) 317–320.
[19] R.S. Rarig Jr., J. Zubieta, Polyedron 22 (2003) 177–188.
[20] X.-B. Cui, K. Lu, Y. Fan, J.-Q. Xu, L. Ye, Y.-H. Sun, Y. Li, H.-H. Yu, Z.-H. Yi, J. Mol. Struct. 743 (2005) 151–155.
[21] R. Xi, B. Wang, K. Isobe, T. Nishioka, K. Toriumi, Y. Ozama, Inorg. Chem. 33 (1994) 833–836.
[22] R.S. Rarig Jr., J. Zubieta, Inorg. Chim. Acta 312 (2001) 188–196.
[23] D. Xiao, H. An, E. Wang, L. Xu, J. Mol. Struct. 738 (2005) 217–225.
[24] E. Burkholder, J. Zubieta, Inorg. Chim. Acta 358 (2005) 116–122.
[25] D. Hagrman, C. Zubieta, D.J. Rose, J. Zubieta, R.C. Haushalter, Angew. Chem. Int. Ed. Engl. 36 (1997) 873–876.
[26] E. Burkholder, J. Zubieta, Solid. State Sci. 6 (2004) 1421–1428.
[27] D.G. Allis, R.S. Rarig, E. Burkholder, J. Zubieta, J. Mol. Struct. 688 (2004) 11–31.
[28] J.-Q. Xu, R.-Z. Wang, G.-Y. Yang, Y.-H. Xing, D.-M. Li, W.-M. Bu, L. Ye, Y.-G. Fan, G.-D. Yang, Y. Xing, Y.-H. Lin, H.-Q. Jia, Chem. Comm. (1999) 983–984.
[29] R.S. Rarig, L. Bewley, E. Burkholder, J. Zubieta, Indian J. Chem. 42A (2003) 2235–2243.
[30] D.G. Allis, E. Burkholder, J. Zubieta, Polyhedron 23 (2004) 1145–1152.

[31] D. Xiao, Y. Hou, E. Wang, S. Wang, Y. Li, L. Xu, C. H, Inorg. Chim. Acta 357 (2004) 2525–2531.
[32] A.J. Bridgeman, J. Phys. Chem. 106 (2002) 12151–12160.
[33] P. Gili, P. Nunez, P. Martin-Zarza, P.A. Lorenzo-Luis, Acta Crystallogr. C 56 (2000) e441–e442.
[34] A.J. Wilson, V. McKee, B.R. Penfold, C.J. Wilkins, Acta Crystallogr. C 40 (1984) 2027–2030.
[35] Q. Li, S.-W. Zhang, Z. Allg, Chem 631 (2005) 645–648.
[36] E.A. Muller, A. Narducci Sarjeant, A.J. Norquist, Acta Crystallogr. E 61 (2005) m730–m732.
[37] M. McCann, K. Maddock, C. Cardin, M. Convery, V. Quillet, Polyhedron 13 (1994) 835–840.
[38] Z.-P. Deng, S. Gao, L.-H. Huo, H. Zhao, Acta Crystallogr. E 61 (2005) m2553–m2555.
[39] J. Gopalakrishnan, Chem. Mater 7 (1995) 1265–1275.
[40] M.T. Pope (Ed.), Heteropoly and Isopoly Oxometalates, Springer, Berlin, Heidelberg, New York, Tokyo, 1983, p. 42.
[41] V.W. Day, M.F. Fredrich, W.G. Klemperer, W. Shum, J. Am. Chem. Soc. 99 (1977) 952–953.
[42] W.G. Klemperer, W. Shum, J. Am. Chem. Soc. 98 (1976) 8291–8293.
[43] M.L. Niven, J.J. Cruywagen, J.B.B. Heyns, J. Chem. Soc. Dalton Trans. 8 (1991) 2007–2011.
[44] T.J.R. Weakley, Polyedron 1 (1982) 17–19.
[45] S.-S. Feng, L.-P. Lu, H.-M. Zhang, S.-D. Qin, X.-M. Li, M.-L. Zhu, Acta Crystallogr. E 61 (2005) m659–m661.
[46] J. Fuchs, H. Harti, Angew. Chem. Int. Ed. Engl. 15 (1976) 375–376.
[47] W. Feng, T. Zhang, Y. Liu, R. Lu, C. Guan, Y. Zhao, J. Yao, Mater. Chem. Phys. 77 (2002) 294–298.